Mon. Not. R. Astron. Soc. **000**, 1–9 (2000) Printed 22 January 2008 (MN LATEX style file v1.4)

A Near Infrared Polarized Bipolar Cone in the CIRCINUS Galaxy

M. Ruiz[1⋆], D. M. Alexander[2], S. Young[1], J. Hough[1], S. L. Lumsden[3], C.A. Heisler[4†]
[1] *Department of Physical Sciences, University of Hertfordshire, Hatfield, Herts AL10 9AB, UK.*
[2] *International School for Advanced Studies, SISSA, Via Beirut 2-4, 34014 Trieste, Italy.*
[3] *Department of Physics and Astronomy, University of Leeds, Leeds LS2 9JT, UK.*
[4] *Mount Stromlo and Siding Spring Observatories, Private Bag, Weston Creek P.O., Weston, ACT 2611, Australia*

22 January 2008

ABSTRACT

We present near–infrared broad–band polarization images of the nuclear regions of the Circinus galaxy in the J, H and K bands. For the first time the south–eastern reflection cone is detected in polarized light, which is obscured at optical wavelengths behind the galactic disk. This biconical structure is clearly observed in J and H band polarized flux whilst in the K band a more compact structure is detected. Total flux J–K and H–K colour maps reveal a complex colour gradient toward the south–east direction (where the Circinus galactic disk is nearer to us). We find enhanced extinction in an arc shaped structure, at about 200pc from the nucleus, probably part of the star-formation ring.

We model the polarized flux images with the scattering and torus model of Young *et al.* , with the same basic input parameters as used by Alexander *et al.* in the spectropolarimetry modelling of Circinus. The best fit to the polarized flux is achieved with a torus radius of ∼16pc, and a visual extinction A_V, through the torus, to the near–infrared emission regions of >66 mags.

Key words: galaxies: active – galaxies: individual (Circinus) – galaxies: nuclei – galaxies: Starburst – infrared: galaxies

1 INTRODUCTION

The investigation of nearby Seyfert galaxies with polarimetric observations provides unique information on the nuclear structure of these objects. This information is of particular importance when studying unification models of Seyfert galaxies.

The standard unified model for Seyfert galaxies proposes that all types of Seyfert galaxy are fundamentally the same, however, the presence of a dusty molecular "torus" obscures the broad line emission in many systems. In this picture the classification of Seyfert 1 or 2 depends on the inclination angle of the torus to the line of sight (Antonucci, 1993). The most convincing evidence for this unified model comes from optical spectropolarimetry. Using this technique, the scattered radiation from the broad line region (BLR) of many Seyfert 2 galaxies is revealed in the form of broad lines in the polarized flux (e.g. Antonucci and Miller, 1985, Young *et al.* , 1996a, Heisler, Lumsden and Bailey, 1997).

Near–IR imaging polarimetry provides valuable information on the nature of the polarizing source (e.g. Lumsden *et al.* , 1999, Tadhunter *et al.* , 1999, Young *et al.* , 1996b, Packham *et al.* , 1996, 1997, 1998, 1999). For example, in NGC1068, bipolar scattering cones are clearly detected in polarized flux (Young *et al.* 1996b, Packham *et al.* 1997) and the torus itself has been viewed in silhouette in the H band (Young *et al.* 1996b). Interestingly, the structure of the scattering cones often coincide with ground-based narrow band imaging (e.g. Wilson and Tsvetanov, 1994) and high resolution HST imaging (e.g. Capetti *et al.* 1997, Falcke, Wilson and Simpson, 1998). Since the unified model infers the presence of a dusty torus obscuring the Seyfert 1 core, we expect that longer wavelength polarimetry will be able to probe deeper into regions within the plane of the torus and to see scattering from the nucleus which might otherwise be shielded from view at optical wavelengths.

Circinus is a nearby (4Mpc) highly inclined (65°, Freeman *et al.* 1977) Sb-Sd galaxy. At this distance, the spatial scale is 20pc/arcsec. It is seen through a low interstellar

⋆ email: mili@star.herts.ac.uk
† We would like to dedicate this work to her memory

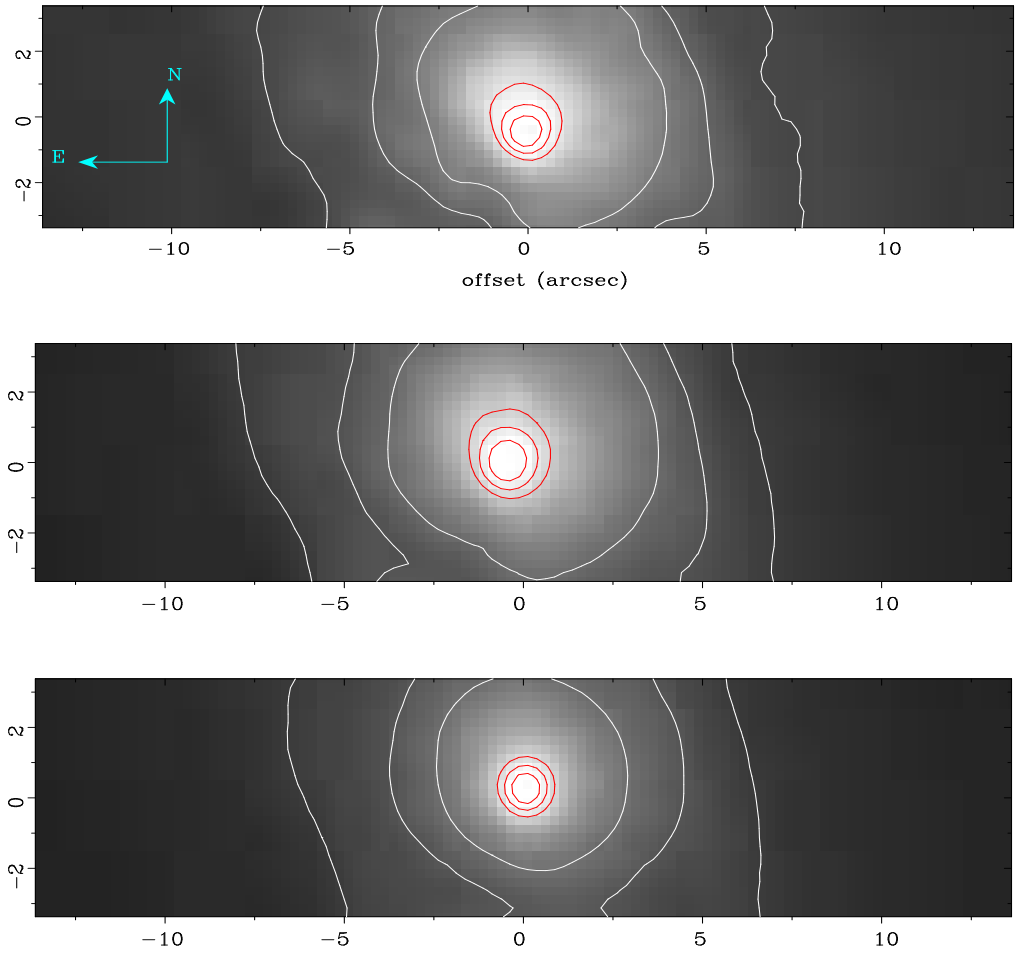

Figure 1. Near-IR images of the Circinus galaxy, J band (top), H band (middle) and K band (bottom). Contours are arbitrarily scaled.

extinction window near the Galactic plane ($A_V = 1.5$ mag; Freeman *et al.* 1977). The nuclear optical line ratios are typical of a Seyfert 2 galaxy. This classification as a type 2 is also supported by the detection of intense coronal lines (Oliva *et al.* 1994), the intense X-ray Fe 6.4 keV line (Matt *et al.* 1996), rapid variation of powerful H_2O maser emission and a prominent ionization cone in [O III]5007 with filamentary supersonic outflows (Marconi *et al.* 1994). Recent optical spectropolarimetry (Oliva *et al.* , 1998 and Alexander *et al.* , 1999a) has shown a scattered polarized broad Hα line and therefore a hidden Seyfert 1 nucleus. Other characteristics include enhanced star forming activity in the form of a star-forming ring of 200pc in size (Marconi *et al.* 1994), a Compton thick nucleus at X-ray energies (Matt *et al.* 1996) and an unresolved nuclear source (<1.5pc) at 2μm (Maiolino *et al.* 1998).

Since it is already known from optical spectropolarimetry that the Circinus galaxy harbours a hidden type 1 nucleus and the optical ionization cone suggests the presence of an obscuring/collimating torus, this galaxy is an ideal candidate to test the theoretical models of unified schemes. The dusty nature of the Circinus galaxy favours near-IR polarimetry over optical polarimetry due to the lower optical depth at near-IR wavelengths.

In this paper we present near–IR imaging polarimetry revealing, for the first time, a biconical emission region. We investigate the nature of this emission in the context of the standard unified model of Seyfert galaxies.

Table 1. Nuclear polarization

Waveband	aperture (arcsec)	%	angle (°)
J	1	2.04±0.38	34.1±3.8
	2	1.71±0.16	38.3 ±2.0
	4	1.40±0.08	46.3±1.1
H	1	2.01±0.15	33.4±2.4
	2	1.75±0.13	35.5±1.9
	4	1.34±0.07	41.1±1.1
K	1	3.25±0.27	32.1±3.1
	2	2.78±0.25	33.7 ±2.9
	4	1.99±0.15	34.7 ±1.8

2 OBSERVATIONS

The data presented here were obtained on the nights of 22 May 1995 (H and K band data) and 11 August 1995 (J band) on the AAT with the common user camera IRIS, which uses

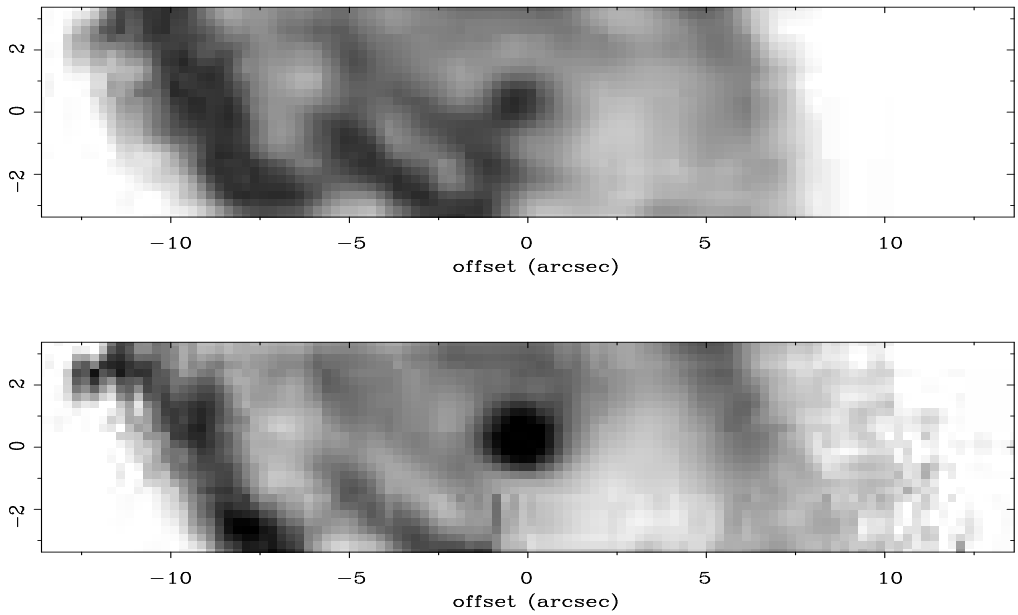

Figure 2. Colour maps of the nuclear regions of the Circinus galaxy. J–K (top) and H–K (bottom). The dark areas correspond to regions of enhanced extinction.

a 128^2 HgCdTe array. We used the cs/36 secondary, which results in a pixel scale of approximately 0.25 arcsec/pixel. The May observations were made under non-photometric conditions. Seeing as estimated in the infrared was $1 - 1.2$ arcsec for the May data, and ~ 0.9 arcsec for the August data. The IRIS photometric standard star SA94-251 was observed at J for the August data. No photometric standards are available for the May data given the conditions. Instead, we used a spectrum of the nucleus of Circinus, taken on 21 Feb 1997 with the echelle grisms inside IRIS, to achieve an overall flux calibration as described below. The stability and instrumental polarization of the instrument were checked using polarized and unpolarized standard stars. The measured instrumental polarization is less than 0.1%, and the instrument is almost completely stable between the two dates when data were taken.

The polarimeter inside IRIS uses a Wollaston beam splitting prism inside the dewar to separate the $o-$ and $e-$rays. A mask in the focal plane prevents the separate images from overlapping. The mask when used with the cs/36 secondary has dimensions on the sky of approximately 30arcsec×8arcsec. A $\lambda/2$ waveplate is positioned in front of the dewar. Each polarimetry dataset is then comprised of exposures at four separate waveplate positions ($0^\circ, 45^\circ, 22.5^\circ$ and 67.5°).

The polarimetry data were reduced as follows. All frames were flatfielded using dome flats. Offset sky frames were taken with varying positions from the nucleus. These frames were median filtered to remove background sources, leaving four separate sky frames for each waveband, corresponding to the four waveplate positions. The four sky frames were scaled to the median level of the sky within each group of four individual object frames, and the result subtracted from the object frames. The resultant images were then registered and combined into separate mosaics for each wave plate position. These final mosaics were combined to form the Q and U Stokes images (using the TSP package and the ratio method – Bailey 1997) and hence polarization maps. Total on-source exposure times for each waveplate position are 960 seconds at J, and 300 seconds at both H and K.

As noted above, the May data were obtained under poor conditions. Therefore, we did not attempt to perform an absolute flux calibration for this data therefore. Instead, we derived relative photometry from the flux-calibrated 1–2.4μm spectrum. This calibration is performed by scaling the J total flux image counts in a circular aperture of equivalent area to that of the spectrum aperture (2arcsec×2arcsec). These counts correspond to the flux as measured in the spectrum at J. The count ratios H/J and K/J as measured from the total flux images are then scaled to the corresponding ratios measured from the spectrum. The main error in this process is in the limited accuracy with which the overall spectral shape is defined. We therefore adopt a conservative error estimate of 30% for the overall flux calibration taken from this data.

3 RESULTS

In this section we present the general results from our data and provide an overview of the features observed in the central regions of the Circinus galaxy. In Fig. 1 we show the J, H and K total flux images of Circinus.

3.1 Colour maps

The J–K and H–K maps are shown in Fig. 2. These maps were generated by registering the peaks of the total flux

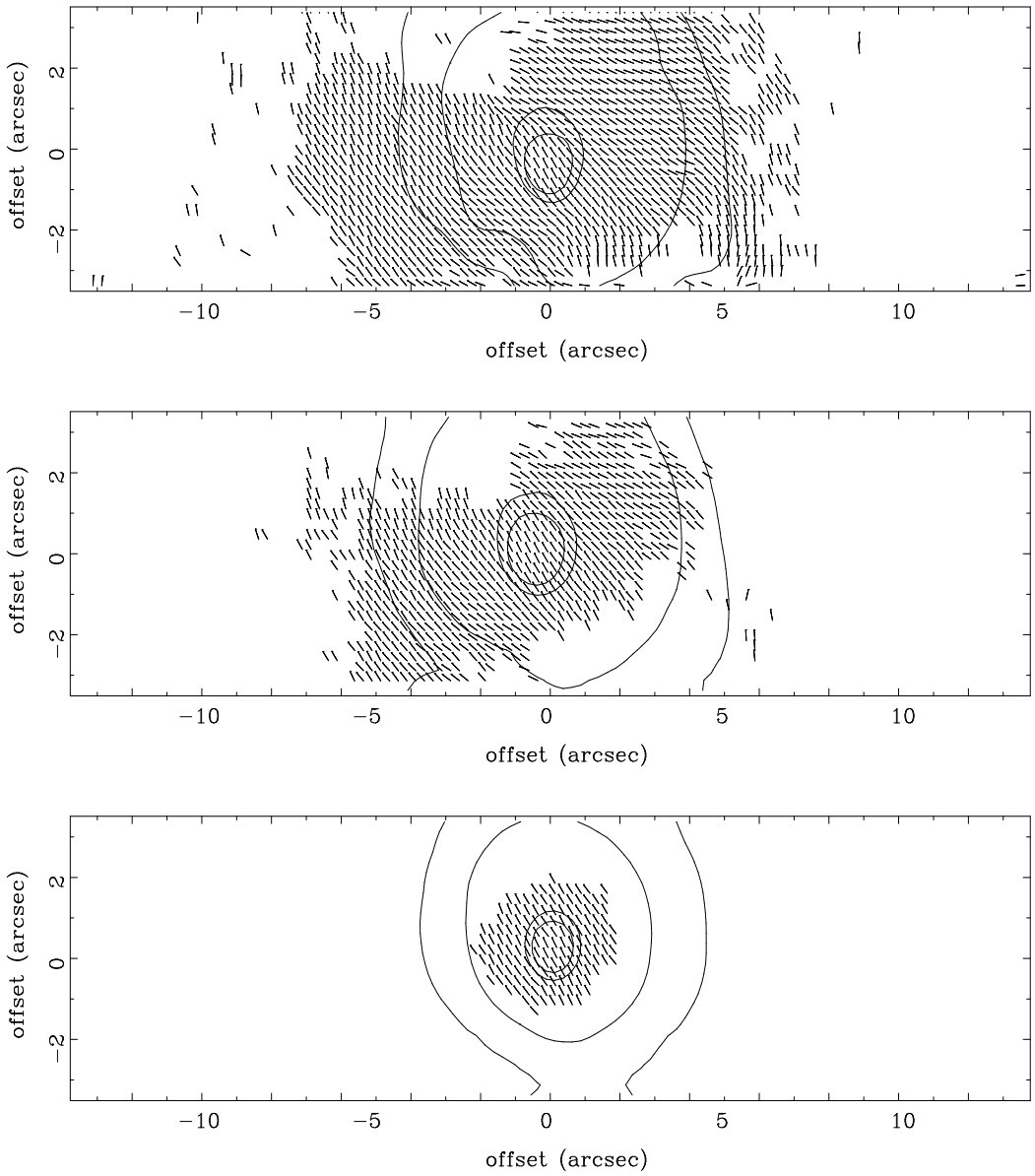

Figure 3. Near-IR polarization maps of Circinus. The J band data is shown at the top, H band in the middle and K band at the bottom. The contours are of the total flux and are arbitrarily scaled. A 1 arcsec polarization vector corresponds to a 10 percent polarization.

images, whose relative offsets did not exceed 2 pixels in RA or DEC. Darker areas correspond to redder colours.

We observe a complex colour structure clearly indicating a non–uniform distribution of dust in the Circinus galactic disk.

In particular, we observe a colour gradient towards the south–east region which is due to an increase in extinction. As discussed by Quillen *et al.* (1995), the closest side of a galaxy disc undergoes the most efficient dust screening, theu, the south-east region of the Circinus galactic disc is closest to us (see also section 4.2).

As previously observed by Maiolino *et al.* (1998), we detect a dust lane close to the nucleus in a bar–like structure, running from the NE to SW which is also connected to the nucleus, best seen in the J–K map. There is another dust lane in a bar–like structure, running parallel to the latter. At about 180pc from the nucleus (9 arcsec), to the East, there is an arc of heavy extinction, which is likely to represent part of the star formation ring previously observed in an Hα image (Marconi *et al.* 1994).

3.2 Polarized maps

The polarization vector maps are shown in Fig. 3, superimposed are the continuum contours. Only those pixels with a level of at least 3σ above the background of polarized intensity are displayed. The J and H polarization vector maps are similar to each other but there is no obvious large–scale symmetry. The highest polarization for J and H is within the 2 arcsec of the nucleus; at J it has a maximum value of 2.04±0.38% at a position angle of 34°± 3.8°and at H it has a maximum of 2.01±0.15% with a position angle

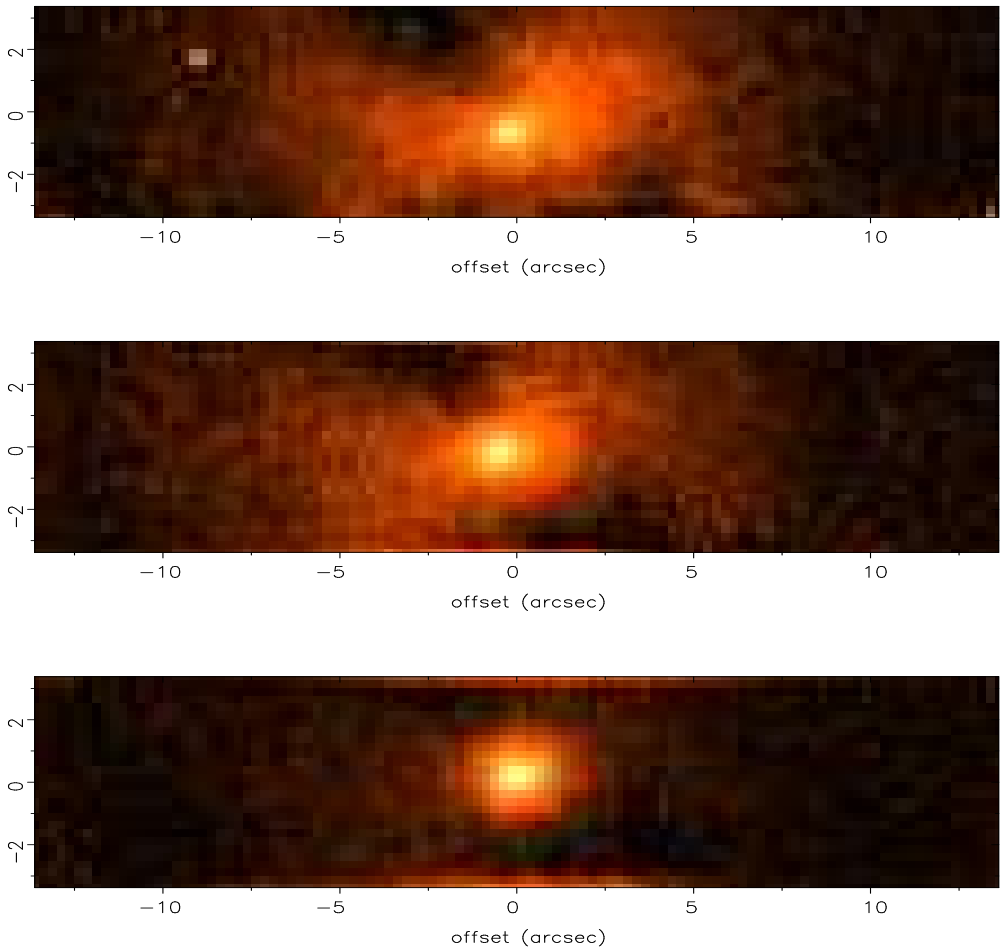

Figure 4. Near-IR polarized flux images of Circinus, J band (top), H band (middle) and K band (bottom), showing the change in polarized structure from predominantly scattering to predominantly dichroism.

of 33.4°±2.4°. The E vectors at K are essentially parallel over the central 5 arcsec with a highest polarization of ∼ 3.25±0.27% at the nucleus a 32°±3°and ∼ 1.6% elsewhere. Table 1 presents polarization and position angle values as measured in various aperture sizes. We notice that the polarization position angle for a nuclear aperture of 1 arcsec is roughly perdendicular to the axis of the infrared scattering cones seen in the J band and the one–sided optical ionization cone (Marconi *et al.* 1994) as well as to the the radio continuum emission (Elmouttie *et al.* 1998). At larger apertures, the polarization position angle changes, due to different contributions to the total polarization such as galactic polarization. The largest change in polarization position angle occurs in the J band. This is because the larger aperture will have contributions from regions dominated by scattering polarization i.e., from the scattering cones. At K, the polarization is dominanted by dichroism (see Section 4) at small and large apertures and the small change in the polarization position angle is likely to be due to galactic polarization.

3.3 Polarized flux images

The near–infrared polarized–flux images are shown in Fig. 4. The J band polarized image shows a double sided cone–like structure, with axis approximately along the NW–SE direction. Previous optical imaging of this galaxy (Marconi *et al.* 1994) showed a one-sided ionization cone in the light of the [O III]5007 line in the north–west direction. More recently, (Maiolino *et al.* 1999) have shown an extended [Si VI]1.95μm emission in the south–eastern region of the nucleus, providing evidence for the existence of a counter–cone, whose existence was previously inferred from radio maps (Elmouttie *et al.* 1995, 1998). Additionally, the presence of polarized emission to the south–east of the nucleus (the "counter–cone") is also indicated by the detection of polarized Hα emission at about 8arcsec to the SE (Oliva *et al.* 1998).

The north–west polarization cone is presumably produced by scattering in a region spatially coincident with the north–west ionization cone. The lack of an ionization cone to the south–east is due to the heavy extinction at optical wavelengths caused by the galaxy disk ($\imath \simeq 65°$), estimated at 5 mags in the visible (Oliva *et al.* 1995; Maiolino *et al.* 1998). In addition, there is evidence for the presence of dust lanes in the south–east direction (Marconi *et al.* 1994; Maiolino *et al.* 1998) and as shown in Fig 2.

As the wavelength of the observations increases, at H and K bands, the bipolar pattern tends to disappear as the

amount of scattered light reduces, as would occur for scattering from small dust grains, and with more nuclear light being seen directly. Fig. 5 shows cuts through the nucleus along the east–west direction of the polarized flux images at J and K, showing the nuclear concentration of the K emission to the central 4 arcsec compared to the more extended J emission.

4 THE SCATTERING MODEL

To model the observed polarization characteristics of the Circinus galaxy, we have used the standard Seyfert model of Young *et al.* (1995), hereafter referred to as the Y95 model.

4.1 Description of the model

The Y95 model takes the standard unification of AGN approach, assuming a bare Seyfert 1 nucleus as the source function for the central source, in this case NGC5548, surrounded by an optically thick torus. The nuclear radiation is collimated by the torus and scattered in a biconical cloud of electrons and/or dust grains. The model also considers the direct view to the emission region, that can be polarized via dichroic absorption by aligned grains within the torus. The model was originally developed to reproduce spectropolarimetric data, and was used to successfully model the polarization of NGC1068 (Young *et al.* 1995), other narrow line active galaxies (e.g Young *et al.* 1996a), and the Circinus galaxy (Alexander *et al.* 1999a). The model was modified to produce images by integrating the scattered intensity over the size of a pixel at the distance of the galaxy in question, as illustrated for NGC1068 (Packham *et al.* 1997).

The most important parameters for the model are the inclination of the cone axis to the line of sight (also the polar axis of the torus in this simple model), the cone half opening-angle, the extinction through the torus to the emission regions and the optical depth to scattering in the cones. The latter is defined in terms of inner and outer scattering radii, a number density of scatterers at the inner radius and the radial dependence of the number density of scatterers. In the case of spatially resolved imaging the inner scattering radius and the radial dependence for the number density also determine the radial scattered light profile with distance from the nucleus.

4.2 Applying the model to the Circinus galaxy

To reduce the number of free variables in the model we can fix some of these parameters. As in the spectropolarimetry modelling of Circinus (Alexander *et al.* 1999a), we set the cone half opening-angle to 45°, which is similar to the observed [O III]5007 emission line cone (Marconi *et al.* 1994). In order to reproduce the intrinsic scattered degree of polarization at 26% (Oliva *et al.* 1995; Alexander *et al.* 1999a) the inclination of the scattering axis to the line of sight is 50°. Except for assuming a large outer scattering radius of 1×10^{20}m, no other assumptions were made prior to the modelling.

The model output images were smoothed with a Gaussian filter with a FWHM chosen to match the seeing of the observations, 1 arcsec for J and H and 1.5 arcsec for K, and then scaled by a factor to match the peak of the polarized image at J. As previously mentioned in section 2, the images are not absolutely flux calibrated but are in suitable units to represent relative fluxes, thus the same scaling factor is used at all wavelengths. Comparisons of the model output with the observations are then made by producing cross–section cuts through the images in the SE–NW direction, in polarized flux. Modelling the polarized flux images, rather than the total flux, to the first order removes the stellar population and the uncertainty of the stellar fraction.

Cross–sections through the observation images, however, show that the polarized nuclear flux has an underlying base, presumably resulting from dichroically polarized stellar emission. This base was fitted separately by a simple addition to the model output. At J this base is consistent with a constant value over the model image size, whilst at H and K the excess was taken as a linearly dependent ramp across the cut. With this pedestal taken into account it is possible to determine the extinction to the scattering regions away from the nucleus. For the south–east scattering cone this is consistent with a visual extinction of $A_V = 5$ mags, while for the north–west cone away from the nucleus, the extinction is $A_V = 1.5$ mags. The latter value of extinction is the same as that determined for the Galaxy (Freeman *et al.* 1977), implying that the south–east scattering cone is actually viewed through an extinction of $A_V = 3.5$ mags arising from the Circinus host galaxy. This value is in agreement with the variation of extinction along the cone–axis measured by Oliva *et al.* (1999), as derived from optical spectral lines.

Two possible orientations for the model were investigated, the first has the less obscured north–west scattering cone pointing towards the observer and the south–east scattering region as the counter–cone, and the second model is the reverse with the forward pointing cone being to the south–east. However, no fit to the observations could be found using the first model and therefore, this case will not be discussed further. Henceforth, the south–east scattering cone is considered to be forward pointing.

To match the radial distribution of the scattered flux from the nucleus, the best fit was obtained with an inner scattering radius of 0.5pc and a radial dependence for the number density of scatterers as r^{-1}. This appears to be tightly constrained, with only a 10 percent alteration in the inner radius being inconsistent with the observations. Unlike NGC1068 (Packham *et al.* 1997), the dichroically polarized direct view to the near–infrared emission region is only readily apparent in the K–band image, which suggests that the extinction through the postulated torus is higher than the $A_V = 37$ mags for NGC1068. However, because we only have one measurement of the direct view, it is not possible to determine absolutely the extinction through the torus for the Circinus galaxy. It is possible to derive a lower limit for this extinction in conjunction with an upper limit for the number density of scatterers. A visual extinction of $A_V = 66$ mags was found to be the lowest compatible with the observations, and the upper limit for the required number density of the scattering electrons at the inner scattering radius were 3×10^{9} m^{-3} for the forward cone and 4.2×10^{9} m^{-3} for the counter–cone. It should be noted that scattering using Rayleigh–type dust grains did not provide a good fit to the observations.

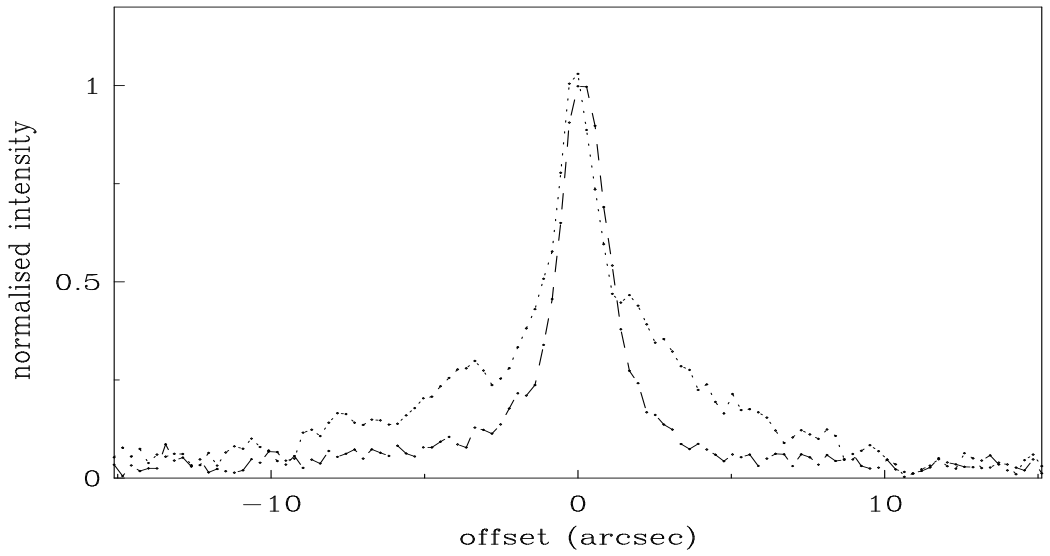

Figure 5. Polarized intensity cuts through the nucleus along the east–west direction for J and K bands. The dashed line represents K and the dotted line represents J. The fluxes have been normalized to unity.

To fully match the cross–sectional cuts through the observations it was necessary to invoke extinction of the scattered flux from the counter–cone by the torus, which was assumed to be an opaque disk. Also, it was found that the best match to the observations was achieved if the galactic extinction of the forward cone extended partially across the counter–cone and dropped off with distance away from the nucleus. The radius of the torus was found to be 16pc, and was well constrained, a smaller torus being inconsistent at J and a larger torus was inconsistent at H. The galactic extinction tail–off was modelled as a simple step, with the full extinction of $A_V = 3.5$ mags stepping down to $A_V = 2.3$ mags to a distance of 25 pc beyond the nucleus in addition to the Galactic extinction of 1.5 mags.

The model parameters are listed in Table 2. Comparison of the cross–sections through the model produce images and the observations in polarized flux are illustrated in Fig. 6 for the J, H and K bands.

Table 2. Model parameters.

Input parameters	
system inclination(°)	50
SE or NW cone opening half-angle(°)	45
SE cone position angle(°)	125
NW cone position angle(°)	305
Best fitting parameters	
inner scattering radius (pc)	0.5
$n_{iscr}(m^{-3})^a$	$< 3 \times 10^9$
$n_{cc}(m^{-3})^b$	$< 4.2 \times 10^9$
α, power law decrement^c	-1
torus radius (pc)	16
A_V through torus	> 66
A_V through galactic disk	3.5
A_V through Galactic disk	1.5

[a] number density at inner radius
[b] number density at counter cone
[c] for number density $\sim r^{\alpha}$

4.3 Discussion

Alexander *et al.* (1999a) modelled the optical and K–band spectropolarimetry data of the Circinus galaxy with scattering, and a dichroic component through the dusty torus corresponding to a visual extinction of $A_V = 35$ mags. In the present study, we have the advantage of being able to constrain the scattered flux with both the spatially resolved information of the images and the extra wavelength coverage with the J and H band images. From this we determine that the ratio of scattered intensity to that from the direct view is higher than that found by Alexander *et al.* (1999a), which explains the difference in the modelled extinction.

We achieved a good fit to our polarized images with a torus radius of approximately 16 pc. This is substantially smaller than the size of the torus determined for NGC1068 of $\sim$ 180 pc (Efstathiou, Hough & Young 1995; Young *et al.* 1996b; Packham *et al.* 1997), but larger than that estimated for Cen A, $\sim$2pc (Alexander *et al.* 1999b).

Modelling the polarized flux images of Circinus only allowed us to place an upper limit for the electron scattering number density, together with a lower limit for the visual extinction through the torus to the near-IR emission region. However, the lower the scatterer's number density, the higher the boost factor (the ratio of the actual luminosity of the source to the observed polarized luminosity). Scattering number densities significantly less than the upper limits, greater than a factor of 10–20, result in a boost factor that, using the scattered broad Hα flux of 4.3×10^{-15} erg

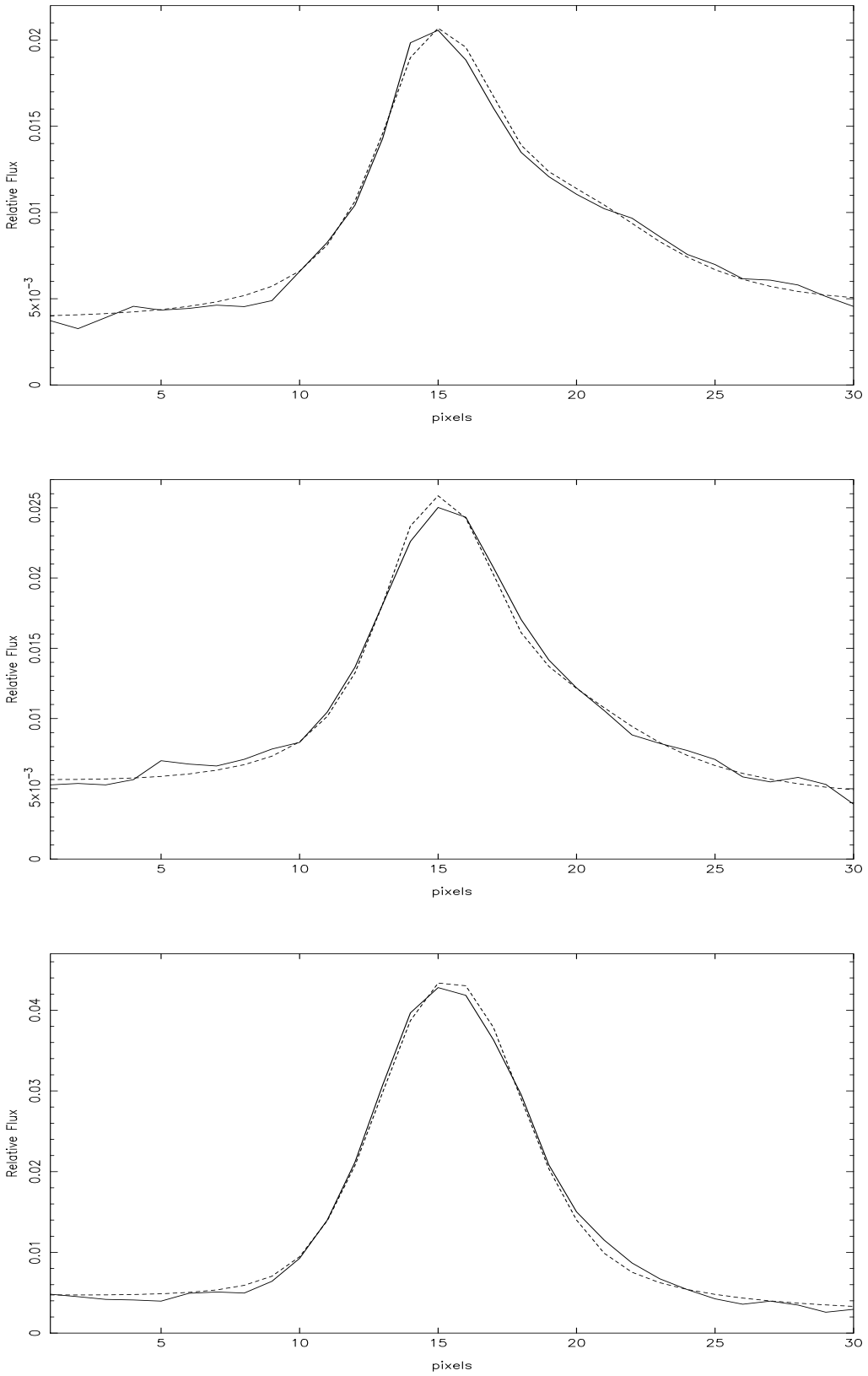

Figure 6. Cross-sections of polarized flux images along the NW–SE direction. J band at the top, H band in the middle and K band at he bottom. The solid line represents the data and the dashed line is the model fit.

s^{-1} cm^{-2} (Alexander *et al.* 1999a), implies a broad Hα luminosity in the top 40 percent of all Seyfert galaxies, while its infrared luminosity is in the lower 20 percent. This argues that the number density of scatterers must be within a factor of 10 of the upper limit.

5 CONCLUSIONS

We have presented near–infrared polarimetric images of the Circinus galaxy showing a clear bipolar scattering cone in the J band. The south–east cone was previously undetected at optical wavelengths because it was hidden behind the heavy extinction of the galactic disk. At longer wavelengths, the H and K band images show more compact structures due to the dominance of dichroic absorption over scattered radiation. We have successfully applied an adapted version of the Y95 model to interpret the observed polarized flux distribution. This model includes two geometrical identical scattering cones, diametrically opposite to each other, with the forward cone in the south–east direction at a position angle of 125° and an opening half angle of 45°. The inclination of the system to the line of sight is 50°. The estimated optical extinction A_V to the nucleus through the torus is >66 mag. We estimate that the putative torus in the Circinus galaxy has an outer radius of ∼16pc.

6 ACKNOWLEDGEMENTS

M.R. thanks PPARC for support through a postdoctoral assistanship. DMA thanks the TMR network (FMRX-CT96-0068) for a postdoctoral grant. We thank Dolores Pérez-Ramírez for her valuable help on the production of this paper.

REFERENCES

Alexander D. M., Heisler C., Young S., Lumsden S., Hough J. H., Bailey J., 1999a, submitted to MNRAS
Alexander D.M., Efstathiou A., Hough J.H., Aitken D.K., Lutz D., Roche P.F., Sturm E., 1999b, MNRAS, 310, 78
Antonucci R., 1993, ARA&A, 31, 473
Antonucci R., Miller J. S., 1985, ApJ, 297, 621
Bailey J.A., 1997, TSP version 2.3. Starlink User Note 66.5
Capetti A., Axon D., Macchetto F. D., 1997, ApJ, 487, 560
Elmouttie M., Haynes R. F., Jones K. L., Ehle M., Beck R., Wielebinski R., 1995, MNRAS, 275, L53
Elmouttie M., Haynes R. F., Jones K. L., Sadler E. M., Ehle M., 1998, MNRAS, 297, 1202
Efstathiou A., Hough J., Young S., 1995, MNRAS, 277, 1134
Falcke H., Wilson A. S., Simpson C., 1998, ApJ, 502, 199
Freeman K. C., Karlsson B., Lygna G., Burrell J. F., van Woerden H. , Goss W.M., Mebold U., 1977, A&A, 55, 445
Heisler C. A., Lumsden S. L., Bailey J. A., 1997, Nature, 385, 700
Lumsden S. L., Moore T. J. T., Smith C., Fujiyoshi T., Bland-Hawthorn J., Ward M. J., 1999, MNRAS, 303, 209
Maiolino R., Krabbe A., Thatte N., Genzel R., 1998, ApJ, 493, 650
Maiolino R., Alonso–Herrero A., Anders S., Quillen A., Rieke M.J., Rieke G.H., Tacconi–Garman L.E., 1999, astro–ph/99101160
Marconi A., Moorwood A. F. M., Origlia L., 1994, Messenger, 78, 20
Matt G., Fiore F., Perola G. C., Piro L., Fink G.G., Grandi P., Matsuoka M., Oliva E., Salvati M., 1996, A&A, 315, L109
Oliva E., Salvati M., Moorwood A. F. M., Marconi A., 1994, A&A, 288, 457
Oliva E., Origlia L., Kotilainen J. K., Moorwood A. F. M., 1995, A&A, 301, 55
Oliva E., Marconi A., Cimatti A., di Serego Alighieri S., 1998, A&A, 329, L21
Oliva E., Marconi A., Moorwood A. F. M., 1999, A&A, 342, 87
Packham C., *et al.* , 1999, in preparation
Packham C., Hough J. H., Young S., Chrysostomou A., Bailey J. A., Axon D. J., Ward M. J., 1996, MNRAS, 278, 406
Packham C., Young S., Hough J. H., Axon D. J., Bailey J. A., 1997, MNRAS, 288, 375
Packham C., Young S., Hough J. H., Tadhunter C. N., Axon D. J., 1998, MNRAS, 297, 936
Quillen A. C., Frogel J. A., Kuchinski L. E., Terndrup D. M., 1995, AJ, 110, 156
Tadhunter C. N., Packham C., Axon D. J., Jackson N. J., Hough J. H., Robinson A., Young S., Sparks W., 1999, ApJ, 512, L91
Wilson A. S., Tsvetanov Z. I., 1994, AJ, 107, 1227
Young S., Hough J., Axon D. J., Bailey J. A., Ward M. J., 1995, MNRAS, 272, 513 (Y95)
Young S., Hough J., Axon D. J., Ward M. J., Bailey J. A., 1996a, MNRAS, 280, 291
Young S., Packham C., Hough J., 1996b, MNRAS, 283, L1

This paper has been produced using the Royal Astronomical Society/Blackwell Science LaTeX style file.